Fingerprint Recognition by Combining Global Structure and Local Cues

Jinwei Gu, *Student Member, IEEE*, Jie Zhou, *Senior Member, IEEE*, and Chunyu Yang

Abstract—As an important feature, orientation field describes the global structure of fingerprints. It provides robust discriminatory information other than traditional widely-used minutiae points. However, there are few works *explicitly* incorporating this information into fingerprint matching stage, partly due to the difficulty of saving the orientation field in the feature template. In this paper, we propose a novel representation for fingerprints which includes both minutiae and model-based orientation field. Then, fingerprint matching can be done by combining the decisions of the matchers based on the global structure (orientation field) and the local cue (minutiae). We have conducted a set of experiments on large-scale databases and made thorough comparisons with the state-of-the-arts. Extensive experimental results show that combining these local and global discriminative information can largely improve the performance. The proposed system is more robust and accurate than conventional minutiae-based methods, and also better than the previous works which implicitly incorporate the orientation information. In this system, the feature template takes less than 420 bytes, and the feature extraction and matching procedures can be done in about 0.30 s. We also show that the global orientation field is beneficial to the alignment of the fingerprints which are either incomplete or poor-qualitied.

Index Terms—Classifier fusion, fingerprint recognition, fingerprint representation, orientation field.

I. INTRODUCTION

NOWADAYS, more and more important applications are based on fingerprint recognition [especially the *automatic fingerprint identification system* (AFIS)] [1], [2], such as electronic personal identification card, e-commerce and various items on the privacy and security of information. These applications often face such a large population that it would probably be a major challenge for the premise of fingerprint identification, i.e., the individuality of fingerprints. In fact, that fingerprint being one kind of testimony has been challenged under *Daubert* in more than 40 court cases to date since the USA versus Byron Mitchell case in 1999 [3]. In most current AFIS systems, only a limited part of discriminative features are utilized [1]. It is believed that incorporating more discriminative information available on fingerprint images into matching stage can strongly reinforce the individuality of fingerprints and improve the performance for fingerprint systems on large scale databases.

Fingerprints are graphical patterns of ridges and valleys on the surface of fingertips. One kind of widely-used features is called *minutiae*, which is usually defined as the ridge ending and the ridge bifurcation. Various methods based on the minutiae-based fingerprint representation were proposed [4], [5]. Despite its simplicity and efficiency in storage, minutiae-based representation has its drawbacks in practical usage. First, as a kind of local features, the minutiae is difficult to be extracted robustly due to various factors such as large displacement, different pressure, noise, etc., especially on the fingerprints with poor quality or collected on the spot. The spurious (falsely extracted) minutiae will degrade the performance seriously [6]. Second, to analyze the individuality of fingerprints, Pankanti *et al.* [7] proposed a mathematical model based on minutiae points with the assumption that minutiae points are independent. Tan and Bhanu [8] extended this work to the two-point or three-point pattern matching and utilized the ridge distance information. Their conclusions also show that only using minutiae points is not strong enough to hold the uniqueness of fingerprints, and incorporating more discriminatory information can largely strengthen this scientific basis for fingerprint recognition.

In last several years, many researchers proposed to use other features for fingerprint matching beside minutiae [1]. Some approaches extracted and used the ridge patterns (shape and frequency) as features for matching [9], [10], and some other methods performed correlation-based matching at the intensity level with the entire images [11], [12]. Recently, Tico and Kuosmanen [13] built a *minutiae descriptor* for each minutiae, which consists of the original minutiae point and a set of local orientation values uniformly sampled around this point. The matching algorithm based on these minutiae descriptors was reported to have better performance than before. Jain *et al.* [6] proposed a novel feature called *FingerCode*. They first detected the reference point and extracted the region of interest around it, then filtered the image with a bank of Gabor filters with different orientations. The filtered results are discretely coded as the feature, and combined with the minutiae for final decision. This method implicitly used the global orientation information. To avoid its sensitivity to the reference point detection, Ross *et al.* [14] proposed to use the entire filtered images, called "ridge feature map," as the features, and combined them with the minutiae as a *hybrid matcher*. All three of these algorithms need large storage for saving the additional features in the fingerprint template, especially the *hybrid matcher* and the *minutiae descriptor*.

The authors are with Department of Automation, Tsinghua University, Beijing 100084, China (e-mail: gujinwei98@mails.tsinghua.edu.cn; jzhou@tsinghua.edu.cn; yangchunyu@mails.tsinghua.edu.cn).

One important kind of features in fingerprints is the orientation field. It is defined as a matrix whose elements are the ridge direction at the corresponding pixel (block) in the original image. The direction is defined in $[0, \pi)$ instead of $[0, 2\pi)$. The orientation field *directly* describes the global structure of the fingerprint ridge pattern. It has been used for image enhancement in the preprocessing stage [15] and fingerprint type classification (indexing) [16]. As a kind of global features, the orientation field has many advantages over the minutiae: 1) it is almost continuous and smooth everywhere except those regions near the singular points, which makes it more robust to be extracted and less sensitive to the noise; 2) compared with the minutiae, it is less sensitive to the image deformation due to the skin condition, the pressure, etc. Few works, as far as the authors know, utilized its discriminant information for fingerprint recognition. This is partly due to the difficulty of storing the entire orientation field in the feature template.

In this paper, we present an intuitive representation for fingerprints which preserves the whole orientation field in the template besides minutiae and other features. On average, it needs less than 420 bytes to store all the information, and feature extraction and matching can be done in about 0.30 s per fingerprint, which makes it suitable for large-scale online processing. It can be extended further by incorporating more features available in the images such as ridge density map. Based on this representation, fingerprint matching is performed by combining the global structure (orientation field) and the local cues (minutiae). We have conducted a set of experiments on two databases (FVC'2002 [1] and THUVLAB), and made thorough comparisons with the state-of-the-arts. Extensive experimental results show that incorporating these local and global discriminant information can largely improve the performance. It shows that our system is more robust and accurate than conventional minutiae-based methods, and it also outperforms the previous methods proposed in [6], [14]. Moreover, we show that the global orientation field can also be used to register the fingerprints which are either incomplete or poor-qualitied (e.g., the latent prints as left on the spot).

The paper is organized as follows. In Section II, we briefly review and analyze several kinds of orientation field models proposed in previous works. In Section III, we propose the fingerprint representation with minutiae and orientation field. The matching algorithm combining both the local minutiae feature and the global orientation field feature is presented in Section IV. The experimental results for fingerprint matching are listed in Section V. Finally, we present another application of the global orientation field for fingerprint alignment in Section VI and conclude in Section VII.

II. MODELS FOR ORIENTATION FIELD

Suppose the orientation field is denoted by $O(x, y)$, most of the models are built on the vector field, $\cos 2O(x, y) + i \sin 2O(x, y)$, which is almost continuous everywhere except at the regions around the singular points (cores and deltas). There are two ways to model a vector field mathematically. One is to directly model it in the complex domain, while the other is to model its real part and imagery part respectively in the real domain.

For the first case, Sherlock and Monro [17] proposed a so-called *zero-pole* model based on the singular points, which takes the core as zero and the delta as a pole in the complex plane. The influence of a core z_c, is $(1/2)arg(z - z_c)$ for point z, and that of a delta z_d, is $-(1/2)arg(z - z_d)$. The orientation at z, is the sum of the influence of all cores and deltas, i.e.,

$$O(x, y) = \frac{1}{2} \arg \left(e^{i\phi} \cdot \frac{\prod_i (z - z_{c_i})}{\prod_j (z - z_{d_j})} \right) \quad (1)$$

where $z = x + iy$, ϕ is a constant to be decided. Vizcaya and GerHardt [18] had made an improvement (called *piecewise-linear* model) using piecewise linear functions around singular points to adjust the zero and pole's behavior. The influence functions are changed to be $(1/2)arg(g_c(z - z_c))$ and $-(1/2)arg(g_d(z - z_d))$ for cores and deltas respectively, where $g_c(\cdot)$ and $g_d(\cdot)$ are piecewise linear functions. The orientation model is then formulated as

$$O(x, y) = \frac{1}{2} \arg \left(e^{i\phi} \cdot \frac{\prod_i g_{c_i}(z - z_{c_i})}{\prod_j g_{d_j}(z - z_{d_j})} \right). \quad (2)$$

Both of these models only depend on the singular points and thus the modeling abilities are rather limited. We have proposed a so-called *rational model* [19] which add some *pseudozeros* and *pseudopoles* as the control points to adjust the original zero-pole model. This rational model is much more general and can also be used when there is no singular point. The formula is as follows:

$$O(x, y) = \frac{1}{2} \arg \left(\frac{\prod_i (z - z_{c_i})}{\prod_j (z - z_{d_j})} \cdot \frac{\sum_m a_m z^m}{\sum_n b_n z^n} \right) \quad (3)$$

where $\{a_m, b_n\}$, $a_m \in \mathbb{C}$, $b_n \in \mathbb{C}$ are the parameters. The pseudozeros are the roots of the additional polynomial in the numerator and the pseudopoles are the roots of the additional polynomial in the denominator.

For the second case, we have proposed a so-called *combination model* [20] which models the real part and the imagery part of the vector field with two bivariate polynomials. To improve the modeling in the noncontinuous regions around the singular points, we impose a point-charge model for each singular point. The formula is as follows:

$$O(x, y) = \frac{1}{2} \arctan$$
$$\frac{\alpha_{PM}(x, y) \sum_{i,j} q_{ij} x^i y^j + \sum_k h_2^{(k)}(x, y) Q_k}{\alpha_{PM}(x, y) \sum_{i,j} p_{ij} x^i y^j + \sum_k h_1^{(k)}(x, y) Q_k} \quad (4)$$

where the parameters are $\{p_{ij}, q_{ij}, Q_k | i = 0, \cdots, N, j = 0, \cdots, N, k = 1, \cdots, K\}$, $p_{ij} \in \mathbb{R}$, $q_{ij} \in \mathbb{R}$, $Q_k \in \mathbb{R}$. $\alpha_{PM}(x, y)$, $h_1^{(k)}(x, y)$, $h_2^{(k)}(x, y)$ are the functions only related to the singular points, which are formulated as

$$\alpha_{PM}(x, y) = \max \left\{ 1 - \sum_{k=1}^{K} \alpha_{PC}^{(k)}(x, y), \quad 0 \right\}$$

where

$$h_1^{(k)}(x,y) = \alpha_{PC}^{(k)}(x,y) \cdot \frac{x - x_0^{(k)}}{r^{(k)}(x,y)}$$

$$h_2^{(k)}(x,y) = \pm \, \alpha_{PC}^{(k)}(x,y) \cdot \frac{y - y_0^{(k)}}{r^{(k)}(x,y)}$$

$$\alpha_{PC}^{(k)}(x,y) = \max\left\{ 1 - \frac{r^{(k)}(x,y)}{r_0^{(k)}}, \quad 0 \right\}$$

and $r_0^{(k)}$ is the effective radius for the k-th singular point which is a predefined constant. $h_2^{(k)}(x,y)$ is "+" if k-th singular point is a core, otherwise is "−." N is the order of the bivariate polynomial, i.e., the highest order term is $x^N y^N$. K is the number of singular points. From the above formulas, the combination model is more general than the other three models and has the strongest ability for modeling. We have shown that this model does have good performance in the computation of the orientation field [21].

III. PROPOSED FINGERPRINT REPRESENTATION

In this section, we propose a fingerprint representation including both the global structure (orientation field) and the local cues (minutiae). As shown in Fig. 1, it contains three parts: the orientation field model, the minutiae (and the singular points if available), and the effective region where the fingerprint ridge pattern exhibits. The minutiae can be extracted by using conventional methods [1], [4], [5], [21]. Only the positions of the minutiae are needed to be stored since the directions of the minutiae can be known from the orientation field model. The effective region, denoted by Ω, is extracted by computing the mean and the variance of the intensity value on each block and doing simple binarization (an *effective* block should have the mean in [2,220] and the variance greater than 6 in our study). A post-processing step including dilation and erosion is made to remove some isolate points and fill large holes. It is then simplified as a P-vertex polygon for storage. These vertexes are defined as the crossing points between the boundary of Ω and the equiangular radial rays from the center of Ω.

We mainly discuss the model-based representation for the orientation field $O(x,y)$ in the rest of this section. To estimate the parameters for the models, first we compute the original orientation field, $O_0(x,y)$, extracted by using the method similar with those in [5], [22]–[24]. After that, *weighted least square* (WLS) method is used to estimate these parameters by *singular value decomposition* (SVD) either in the complex domain for the rational model [19], or in the real domain for the combination model [21]. For numerical stability, the coordinates of (x,y) are normalized into $[-1,1]^2$ with the origin centered in the image. In practice, researchers usually compute the orientation value for each $w \times w$ block instead of each pixel [1]. In all of our experiments, w is set as 4 pixels empirically, and $r_0^{(k)} = 60$ pixels if the k-th singular point is a core and 40 pixels for a delta.

As shown in (3) and (4), both of these models require the singular points beforehand. However, it is not easy to detect the singular points robustly and accurately [6], [21], especially in some poor-qualited fingerprints with creases, scars, etc. In the
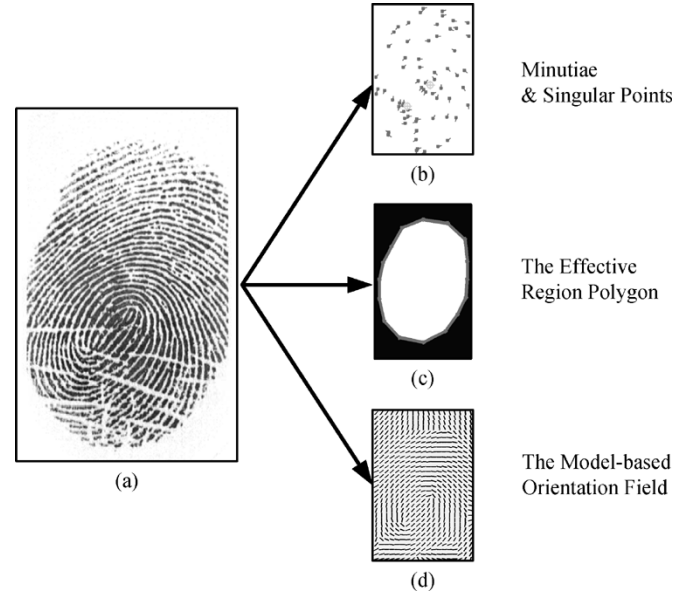

Fig. 1. Fingerprint representation with global and local features. (a) original image, (b) minutiae and singular points, (c) polygon-based effective region, and (d) model-based orientation field.

case that singular points are not available for detection at all, two modified models can be used, which are formulated as

$$O(x,y) = \frac{1}{2} \arg \frac{\sum_m a_m z^m}{\sum_n b_n z^n} \tag{5}$$

and

$$O(x,y) = \frac{1}{2} \arctan \frac{\sum_{i,j} q_{ij} x^i y^j}{\sum_{i,j} p_{ij} x^i y^j}. \tag{6}$$

They are denoted as *rational model II* and *combination model II*. As expected, these models will not perform as well as the former ones at the regions around the singular points. But they have less parameters and are more robust when the singular points can not be detected satisfactorily.

The required storage for this representation is rather small. It costs $2P$ bytes to store the P-vertex polygon for Ω. For the orientation field model, there is $2(N+1)^2 + K$ coefficients for the combinational model and $2N+1$ coefficients for the rational model (in the complex domain), where N is the polynomial's order and K is the number of singular points. We have analyzed the numerical rounding-off errors and proved that 4 bytes are accurate enough for storing each parameter. Besides, it costs $2K$ bytes and $K/8$ bytes to store the positions and the types of the singular points, respectively. The minutiae need $2M$ bytes to store their positions, where M is the number of the minutiae. The total storage for this representation will be

$$2(N+1)^2 \cdot 4 + K \cdot 4 + 2K + \frac{K}{8} + 2P + 2M. \tag{7}$$

For most fingerprints, $K \leq 4$ (i.e., two cores and two deltas), and the average minutiae number for one fingerprint, M, can be assumed to be less than 80 [1], [2], [7]. N and P are set empirically as $N = 4$, and $P = 16$. Therefore, we need at most **417** bytes for storing the minutiae, the whole orientation

field, the effective region and the singular points. This storage is much smaller than that in previous works (see Table III for details) while we record more information available in fingerprint images. The features can be extracted in real-time (about 0.30 s per fingerprint without optimization). Finally, we would like to emphasize that: after modeling, the orientation field is more stable and resistant to noise [21], and thus the discriminatory information is expected to be strengthened instead.

IV. FINGERPRINT MATCHING

In this section, we describe fingerprint matching by combining both the local cue (minutiae) and the global structure (orientation field). For two given fingerprints denoted with $\mathcal{A}$ and $\mathcal{B}$, we assume that they have already been aligned properly with the minutiae features (details about the alignment algorithms are referred to Section VI). The intersection of the effective regions can be defined as $\Omega = \Omega_{\mathcal{A}} \cap \Omega_{\mathcal{B}}$. We first discuss the matching only based on the orientation field, and then discuss how to combine it with conventional minutiae-based matching algorithms. To compare different orientation models, similarity functions, and fusion strategies, we have carried a set of experiments on a training database (see Section V for details). The definitions of performance measurements are given as follows.

If the two fingerprints of a given matching are from a same finger, it is a *genuine matching*, otherwise an *imposter matching*. The performance of a biometric system operating in a verification mode can be specified in terms of *false acceptance rate* (FAR) and *false rejection rate* (FRR). Given a threshold, FAR is defined as the percentage of those imposter matchings whose scores are greater than the threshold, and FRR is defined as the percentage of those genuine matchings whose scores are less than the threshold. The *receiver operating curves* (ROC) plotting FAR versus FRR under different thresholds is often used to evaluate the system's performance. A practical decision scheme is usually established to choose a threshold which minimizes FRR while keeping a given FAR.

The major challenge for various fingerprint verification algorithms is how to reduce FRR when FAR is lower than a required value. For simplicity, we denote $\mathrm{FRR}_{\alpha\%}$ as the value of FRR when $\mathrm{FAR} = \alpha\%$. The typical values we are concerned about are $\mathrm{FRR}_{0.01\%}$, $\mathrm{FRR}_{0.1\%}$ and $\mathrm{FRR}_{1\%}$. These values, generally speaking, are more meaningful than the *equal error rate* (EER) in practical AFIS systems (e.g., in a real fingerprint verification system for high security such as military organizations, it is a standard requirement that FAR should be lower than 0.01% [2]).

A. Matching Based on Orientation Field

The similarity (matching score) between the orientation fields of $\mathcal{A}$ and $\mathcal{B}$ is defined as

$$S(\mathcal{A}, \mathcal{B}) = \frac{1}{|\Omega|} \int\int_{(x,y)\in\Omega} s\left(\delta(x,y)\right) \qquad (8)$$

where $|\Omega|$ is the area of the intersection of the effective regions, and $s(x)$ is a similarity function defined in $[0,1]$. $\delta(x,y)$ is the normalized difference between the orientation

TABLE I
RESULTS WITH DIFFERENT SIMILARITY FUNCTION $s(x)$ DEFINITION

$s(x)$	$\mathrm{FRR}_{0.01\%}$	$\mathrm{FRR}_{0.1\%}$	$\mathrm{FRR}_{1\%}$	EER
$\exp(-10x)$	41.0%	22.1%	10.9%	6.4%
$u(x) - u(x-0.1)$	45.1%	25.7%	12.6%	6.5%
$1-x$	52.9%	29.3%	13.3%	6.6%

values at the point (x,y) in $O_{\mathcal{A}}$ and $O_{\mathcal{B}}$, which is formulated as follows:

$$\delta(x,y) = \begin{cases} \frac{2}{\pi}\delta_0(x,y), & \text{if } \delta_0(x,y) \le \frac{\pi}{2} \\ \frac{2}{\pi}\left(\pi - \delta_0(x,y)\right), & \text{otherwise} \end{cases} \qquad (9)$$

where

$$\delta_0(x,y) = |O_{\mathcal{A}}(x,y) - O_{\mathcal{B}}(x,y)|.$$

Selecting Similarity Function: To estimate the optimal similarity function $s(x)$, we use the method similar with that in [13]. The optimal $s(x)$ is defined as the one that maximizes the similarity between the matched fingerprints while minimizing the similarity between the nonmatched fingerprints. It can be formulated as follows:

$$s^* = \arg\min J(s) = \frac{\left(\int_{x=0}^1 s(x)p(x|\mathcal{H}_1)dt\right)^2}{\left(\int_{x=0}^1 s(x)p(x|\mathcal{H}_0)dt\right)^2} \qquad (10)$$

where $\mathcal{H}_0$ is the hypothesis that the two blocks with the normalized orientation distance x are not corresponded (i.e., nonmatched), and $\mathcal{H}_1$ is the hypothesis that they are corresponded (i.e., matched). $p(x|\mathcal{H}_1)$ and $p(x|\mathcal{H}_0)$ are the corresponding conditional probability density functions (p.d.f), which can be estimated on the training database. Based on the observation that $p(x|\mathcal{H}_0)$ is nearly the uniform distribution and $p(x|\mathcal{H}_1)$ is almost the exponent distribution, as in [13], the optimal similarity function can be derived as

$$s(x) = kp(x|\mathcal{H}_1) = \exp\left(-\frac{x}{\mu}\right) \qquad (11)$$

where k is a constant. The mean μ is set as $1/10$ empirically, and thus $s(x) = \exp(-10x)$.

We have compared the above function with several other similarity function definitions on the training database. Table I shows the performances of the *combination model* based orientation field classifier using different similarity functions. The results show that the exponent function, $\exp(-10x)$, works best, and thus it is chosen for all of the experiments in this paper. The same conclusion can also be drawn for the other kinds of orientation field models.

Selecting Orientation Field Model: We have compared the performances of the classifiers combining minutiae and orientation field using different models, including *zero-pole model*, *piecewise linear model*, *combination model*, *rational model*, *combination model II* and the *rational model II* on the training database. The ROC curves are shown in Fig. 2. We have tried
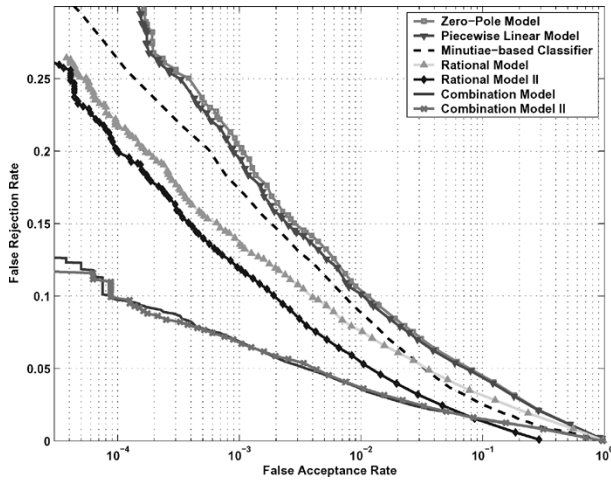
Fig. 2.   ROC curves for the classifiers combining minutiae and orientation field using different models.

all of classifier fusion strategies mentioned below and selected the best ROC curve for each model.

The experimental results show that *combination model* and *combinational model II* have the best performance. *Rational model* and *rational model II* also have satisfactory performance than the conventional minutiae-based classifier. *Zero-pole model* and *piecewise linear model* do not perform well. The reason we found is that these models rely heavily on singular points detection. Falsely detected singular points often occurs on the images which are seriously blurred or containing a lot of creases in the databases. Although *combination model* is also related to the singular points, it can tolerate false singular points detection in some sense [21], so that it still can have good performance.

Original Orientation Field versus Model-Based Orientation Field: Despite the storing advantage of the model-based orientation field representation, it is interesting to study the influence of the modeling procedure on the discriminatory information of the orientation field. Two matching experiments are carried on the training database, one of which used the extracted *original* orientation fields while the other used the *model-based* reconstructed orientation fields with *combination model*.

Fig. 3 showed the distributions of the orientation field matching scores. The Kullback-Leibler divergence of the distributions of genuine and imposter matching for the *original* orientation fields is 5.70, and that of the model-based orientation fields is 6.89. In Fig. 4, we showed the ROC curves of the classifier only using the orientation field and the classifier combining both minutiae and orientation field. For the latter classifier, we have tried all of fusion strategies mentioned below and selected the best ROC curve for each case. These results show that the *model-based* orientation fields contain more discriminant information than the *original* orientation fields, and thus have better recognition performance. Although it might not be as accurate as the *original* orientation field in some places, the *model-based* reconstruction is more robust and more suitable as a kind of feature. Nevertheless, we found that not every model is more discriminant than the original one, and the *combination model* is the best.
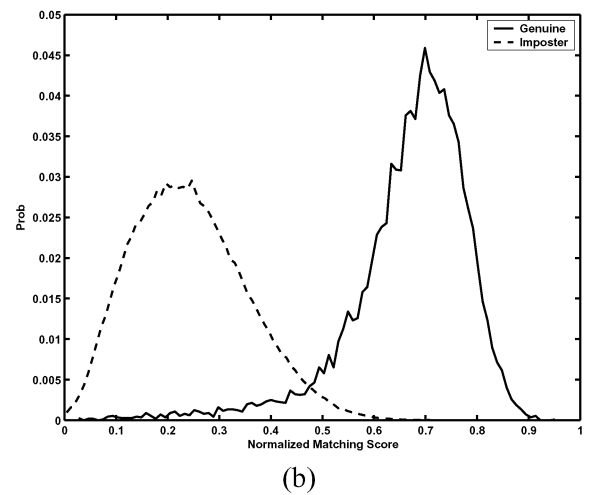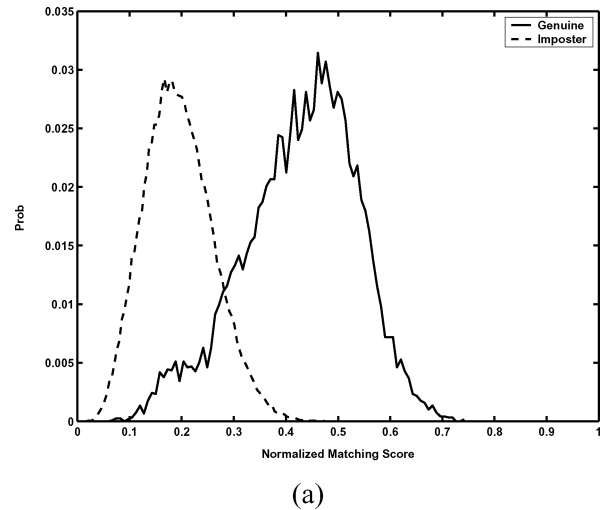

(a)

(b)

Fig. 3.   (Solid line) Distributions of the matching scores for genuine matching and (dash line) imposter matching, with the classifier only using (a) the *original* orientation field, and (b) the *model-based* orientation field with the *combination model*.

B. Matching by Combining the Features

Although the global orientation field information is discriminant, it is not enough to identify those fingerprints which are similar globally while different in details, such as the prints from twins' fingers. One natural way to overcome this problem is to combine the orientation field with the conventional minutiae for fingerprint recognition, as shown in Fig. 5.

Minutiae-Based Fingerprint Matching: Before combining the matchers, we briefly review the minutiae-based matching algorithms. Most of the minutiae-based approaches count the number of the matched minutiae pairs in Ω, and normalized it with the minutiae numbers of each fingerprints to get the matching scores [4], [5], [13]. Two minutiae points are regarded as *matched* when: 1) the differences of their coordinates are less than Δ_x and Δ_y for x axis and y axis, respectively, and 2) the angular difference between their directions does not exceed Δ_θ. Δ_x, Δ_y and Δ_θ are the constants determined by the experiments. In our study, their values are set as ten pixels, ten pixels, and 0.175, respectively. Denote the numbers of the minutiae in Ω are $N_\mathcal{A}$ for the fingerprint $\mathcal{A}$, $N_\mathcal{B}$ for the fingerprint $\mathcal{B}$,
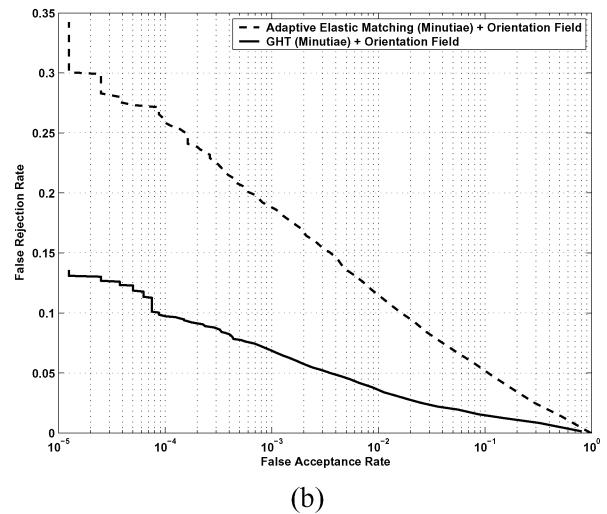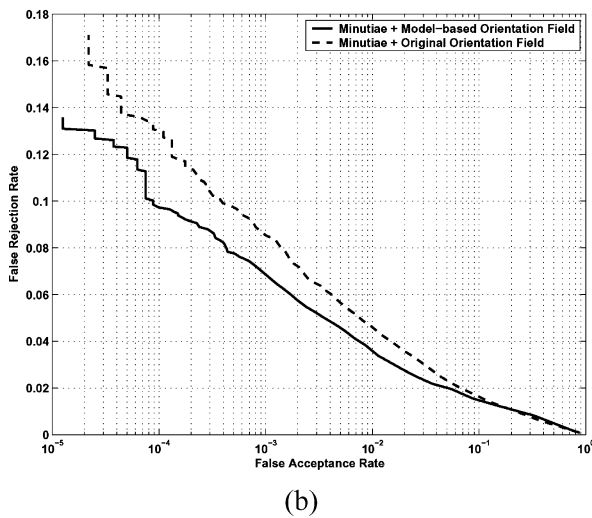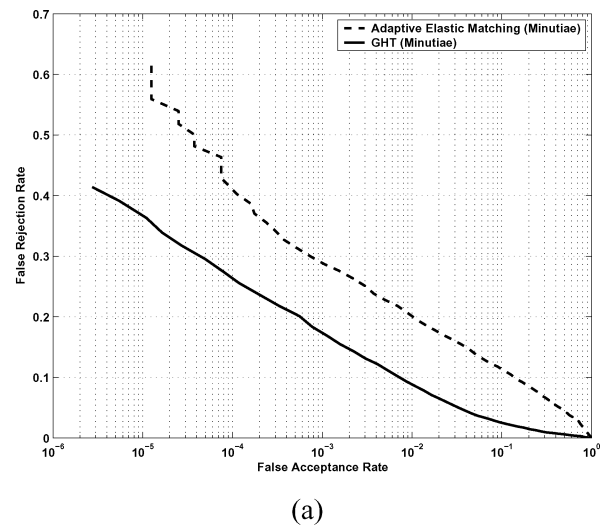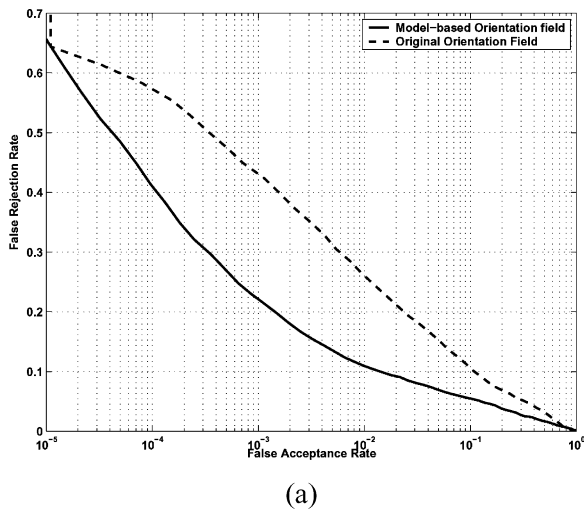
(a)

(b)

Fig. 4.   ROC curves of the classifier using (a) the orientation field only and (b) the classifier combining both minutiae and orientation field, with the *original* orientation field (dash line) and the *model-based* orientation field (the *combination model*).

(a)

(b)

Fig. 6.   ROC curves of the classifier using (a) the minutiae only and (b) combining both minutiae and orientation field, with the GHT method (solid line) and the adaptive elastic matching algorithm (dash line).
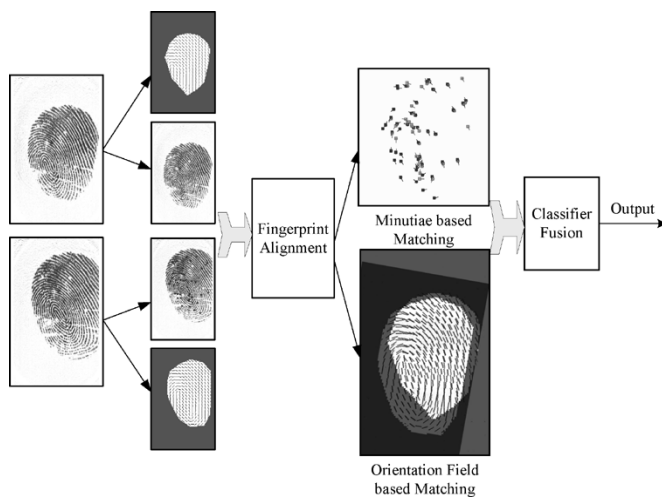
We have implemented two representative minutiae-based matchers, and fused the orientation-field-based matcher with each of them. One is the general Hough transformation (GHT) method [4]; the other is the *adaptive elastic matching* algorithm [5]. The latter one transforms the minutiae sets of two fingerprints into polar coordinates, then sorts them into two "strings" by the angles, and adopts the elastic string matching algorithm for minutiae matching.

In Fig. 6, we showed the ROC curves on the training database of the two minutiae-based matchers and their combinations with a same orientation-field-based matcher (using the *combination model*). We have tried all of fusion strategies mentioned below and selected the best for each case. The results show that: 1) combining with the orientation field information can largely improve the performance, either for the GHT minutiae matcher or the *adaptive elastic* matcher; 2) the GHT minutiae-based matcher, although simple, has better performance than the *adaptive elastic matching* method on our database.

Classifier Fusion: Many methods have been proposed [25], [26] for classifier fusion, which can be mainly classified into three categories: 1) the heuristic rule-based methods such as

Fig. 5.   Flowchart of the proposed combination system.

and N for the *matched* minutiae points. The matching score is usually computed as $(N^2/N_{\mathcal{A}}N_{\mathcal{B}})$.

SUM, MIN, MAX, Major Voting, etc. as listed in [25]; 2) the distribution-based methods such as Neyman–Pearson's rules [6], [27]; and 3) the *stacking* method that trains a suffixal classifier whose inputs are the outputs of the classifiers to be fused [28]. In our study, two classifiers (minutiae-based matcher and orientation-field-based matcher) need to be combined. We have implemented and compared several strategies for each category with experiments.

For the heuristic rule category, we implemented the SUM, MIN, and MAX rules. As pointed out in [25], when there are only two classifiers to be fused, these three rules are enough to represent all other fusion rules such as PRODUCT or Major Voting. For the stacking category, we implemented a method to train an one-hidden-layer back propagation neural network (*BP Net*) as the stacking (fusion) classifier. The number of the hidden units is set to 5 empirically.

As for the second category (the distribution-based methods), we have implemented several approaches. Suppose the joint genuine class-conditional density is denoted by $p(X_1, X_2|w_G)$ and the joint imposter class-conditional density is denoted by $p(X_1, X_2|w_I)$, where X_1 and X_2 denote the matching scores for the minutiae-based classifier and the orientation field based classifier, respectively. The Neyman–Pearson rule, which is the optimal rule under the Bayesian meaning [29], is formulated as follows:

$$(X_1, X_2) \in \begin{cases} w_G, & \text{if } \frac{p(X_1, X_2|w_G)}{p(X_1, X_2|w_I)} > \lambda \\ w_I, & \text{otherwise.} \end{cases} \quad (12)$$

Jain *et al.* [6] assumed that X_1 and X_2 are independent stochastic variables, thus the joint density function can be computed as the product of the two one-dimensional (1-D) distributions

$$\begin{cases} p(X_1, X_2|w_G) = p(X_1|w_G)p(X_2|w_G) \\ p(X_1, X_2|w_I) = p(X_1|w_I)p(X_2|w_I). \end{cases}$$

We refer this method as *1-D Neyman–Pearson*. A more general method is to directly estimate the two-dimensional (2-D) distributions such as the one proposed in [27] using 2-D Parzen Window. In order to get more precise performance, instead, we use 2-D Gaussian mixture model (GMM) to estimate the 2-D distributions directly. The number of the Gaussian kernels are set to 5 empirically for both distributions. We use the expectation maximization (EM) algorithm to estimate the parameters of the GMM [30]. We refer this method as *2-D Neyman–Pearson*.

Among the above classifier fusion strategies, *1-D Neyman–Pearson*, *2-D Neyman–Pearson*, and *BP net* need a training step. We have evaluated all these classifier fusion strategies on the training database. Their performances, along with those of the two separate classifiers, are given in Table II. It shows that: 1) all of the combined classifiers, except the MAX rule, are better than either of the separate classifiers. $\text{FRR}_{0.01\%}$ for the combined classifier can reach 9.7%, while 26.4% for that of the minutiae-based classifier and 41.0% for the orientation field based classifier, and 2) SUM has the best performance among all these strategies. The *1-D Neyman–Pearson* also works quite well. But note that this is the training result for *1-D Neyman–Pearson*, and it can not perform as good on the testing database. On the other

TABLE II
RESULTS WITH DIFFERENT CLASSIFIER FUSION METHODS

	$\text{FRR}_{0.01\%}$	$\text{FRR}_{0.1\%}$	$\text{FRR}_{1\%}$	EER
SUM	9.7%	6.8%	3.6%	2.5%
MIN	12.4%	8.2%	4.5%	3.1%
MAX	33.1%	14.6%	7.4%	4.8%
Neyman-Pearson 1D	10.2%	8.4%	4.0%	2.9%
Neyman-Pearson 2D (GMM)	14.0%	9.9%	5.6%	3.3%
BP Net	13.6%	11.1%	7.0%	3.5%
Only Minutiae (No Fusion)	26.4%	17.4%	8.8%	4.3%
Only Orientation Field (No Fusion)	41.0%	22.1%	10.9%	6.4%

hand, SUM does not need a training step, and thus its performance will remain a high level in different database. Therefore, we choose this fusion strategy for the rest experiments.

V. EXPERIMENTAL RESULTS

This section is organized as follows. First, the databases used in this paper are described. Second, we show the experimental results of fingerprint matching by combining the minutiae and the model-based orientation field. Finally, the comparisons between our algorithm and some representative previous works are presented.

A. Fingerprint Databases

There are two databases used in this paper. The first one, called THUVLAB, is collected from 191 nonhabituated cooperative subjects using a Digital Persona optical sensor. The image size is 512×320 pixels with 500 dpi and 256 gray levels. Among these subjects, 67.2% are younger than 25; 25% are between the ages of 25 and 50; 7.8% are older than 50. Approximately 20% of the subjects were female. The total number of fingers we collected is 827. Each finger was pressed eight times in different days, and thus the whole database consists of $827 \times 8 = 6,616$ fingerprints. During the data acquisition process, we did not supervise or assist the subjects in order to simulate the real situation as best as possible. Therefore, there is a significant intra-class deformation for many fingerprints, mainly due to the large translation (up to ± 200 pixels, average ± 80 pixels) and rotation (up to $\pm 45°$, average $\pm 20°$) and serious finger pressure differences. The fingerprint images in THUVLAB vary in qualities and types. More than 30% are suffering the affection from deformity, incompleteness, large creases, scars and smudges in the ridges or dryness and blurs of the fingers. Some fingerprint samples are listed in Fig. 7.

We randomly selected 400 fingers as the *training database*, and used the remaining 427 fingers as the *testing database*. As mentioned in Section IV, the training database is used to compare different orientation models, similarity functions and fusion strategies. The testing database is used to evaluate the proposed algorithm and compare it with the previous state-of-the-arts. For each finger, each two of its eight prints are matched. This generates $\binom{8}{2} \times 427 = 11\,956$ *genuine* matchings. Considering the efficiency, for two different fingers, we randomly selected two matchings from 8×8 matchings between them, and thus generated $2 \times \binom{427}{2} = 181\,902$ *imposter* matchings.
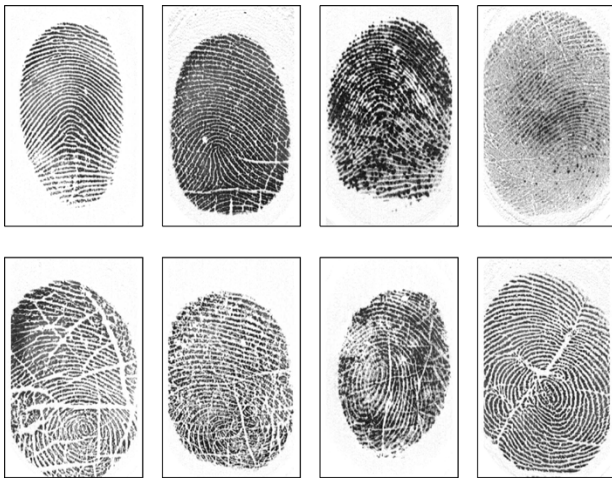
Fig. 7.   Sample fingerprint images in THUVLAB database with various types and quality.
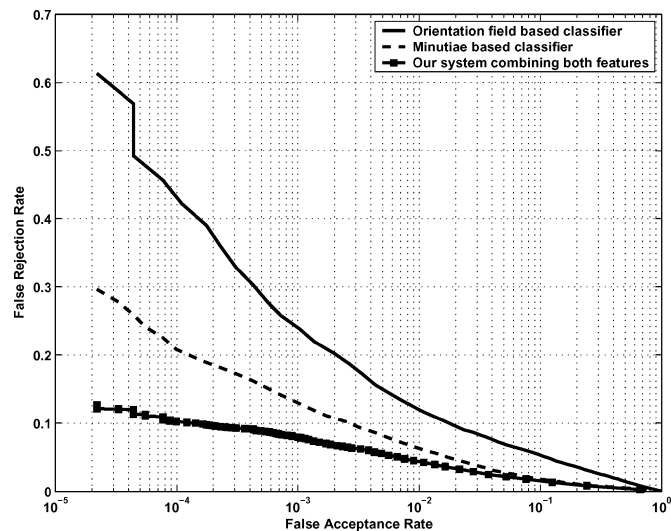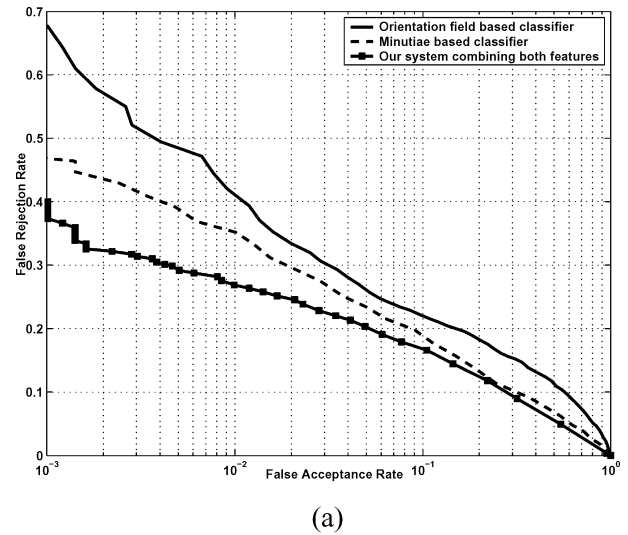

(a)

Fig. 8.   ROC curves on the testing database of THUVLAB for the minutiae-based classifier (dash line), the orientation-field-based classifier(solid line), and our proposed algorithm (marker line) by combining both the orientation field and the minutiae.

(b)

Fig. 9.   ROC curves on FVC'2002 (DB3 and DB4) for the minutiae-based classifier (dash line), the orientation-field-based classifier(solid line), and our proposed algorithm (marker line) by combining both the orientation field and the minutiae.

The second database is FVC'2002 [1], which consists of four collections and each one contains $110 \times 8 = 880$ images. As reported, DB3 and DB4 are generally much more difficult for conventional minutiae-based matchers than the other two collections. Therefore, we tested our proposed algorithm on DB3 and DB4 using the experimental protocols proposed in [31].
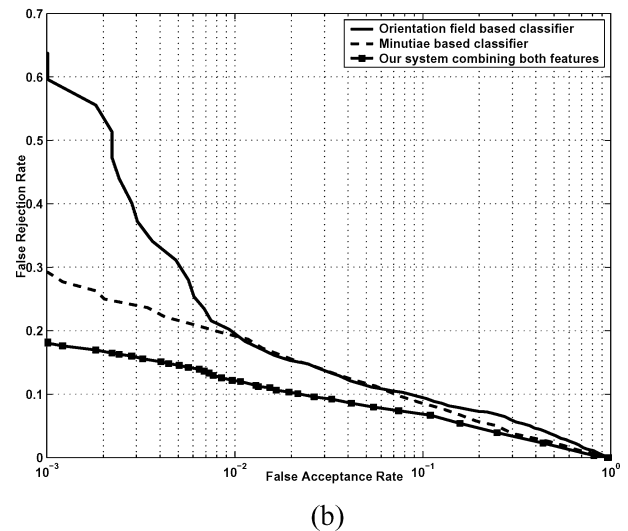
All the algorithms presented in this paper are implemented with C++ on a AMD 2200 Hz 512M PC computer, and the time costs are all estimated on this computer.

B. Matching by Combining Minutiae and Orientation Field

The ROC curves of our proposed algorithm are shown in Fig. 8 (on the testing database of THUVLAB), and Fig. 9 (on FVC'2002 database). The ROC curves of the minutiae-based classifier, and those of the orientation field based classifier are also shown for comparison. As pointed out in the previous section, we use the GHT minutiae-based classifier, and the model-

based orientation field classifier (with the *combination model*). The fusion strategy is the SUM rule.

The results show that combining both the global structure and the local cues will largely improve the performance. These two kinds of features complement each other. As we expected, the orientation field based classifier does not perform as well as the conventional minutiae based classifier. By analyzing the results, we found that most of the false accepts of the orientation-field-based classifier occur among the same type (class) of fingerprints, which confirms our assumption that the orientation field captures the global structure information more than the local details.

In Fig. 10, we presented the distributions of (X_1, X_2) for all genuine and imposter matchings on the testing database of THUVLAB. We have computed the correlation coefficients between the matching scores of the minutiae based classifier, X_1, and those of the orientation field based classifier, X_2. The correlation coefficients are 0.53 for the genuine matchings and 0.14 for the imposter matchings, which indicates that the local feature (minutiae) and the global structure (orientation field) are
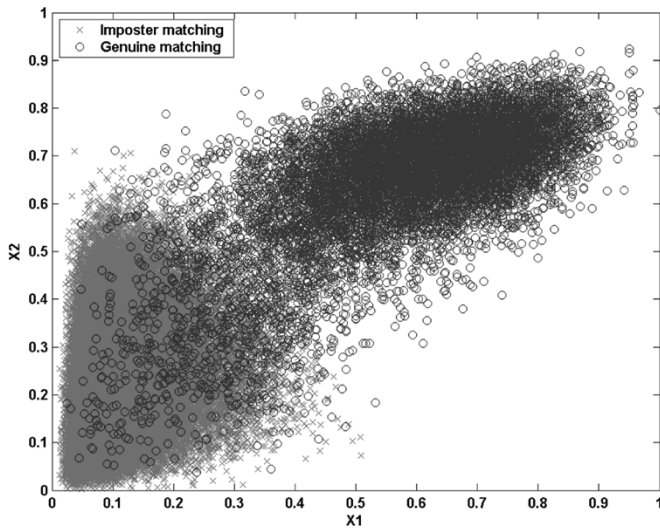
Fig. 10. Distributions of (X_1, X_2) for genuine and imposter matchings on the testing database of THUVLAB, where X_1 is the normalized matching score of the minutiae-based classifier and X_2 is the normalized matching score of the orientation-field-based classifier.

rather independent. The same conclusion can also be drawn on FVC'2002 database.

C. Comparison With Previous Works

We have compared our system with two representative works which also implicitly adopt some orientation information into the fingerprint matching stage: *Algorithm A*, the *FingerCode*+Minutiae method [6], and *Algorithm B*, the *Hybrid matcher* [14]. We have carefully implemented these algorithms and tuned the parameters. The minutiae extraction method is the same for all of tested systems for fair comparison.

Different with *Algorithm A* and *Algorithm B*, our approach explicitly uses the model-based orientation field instead of several Gabor-filtered images (or "ridge feature map" in *Algorithm B*). Besides less storage and computational cost, one advantage of our approach is that the model-based orientation field has intuitive physical meaning and is more robust to noises.

First, in Fig. 11(a), we present the ROC curves on the testing database of THUVLAB of the classifier only using the *FingerCode*, that of the classifier only using the ridge feature map in the *hybrid matcher*, and that of the classifier only using the model-based orientation field. It shows that: 1) the model-based orientation field is better than the *FingerCode* and the ridge feature map when $\mathrm{FAR} > 0.01\%$, and 2) the ridge feature map is slightly better than the *FingerCode*, since it is more robust without detecting the reference point.

Second, by combining with the minutiae-based matcher, we have compared the proposed algorithm with *Algorithm A* and *Algorithm B* in Fig. 11(b). The ROC curves show that our approach, combining the minutiae and the model-based orientation field, achieves the best performance. Both these comparison experiments have also been carried on FVC'2002 database, and the same conclusions can be drawn.

Finally, some detailed comparison including the requirements of the feature template storage and the processing time are listed in Table III. The average minutiae number of each fingerprint,
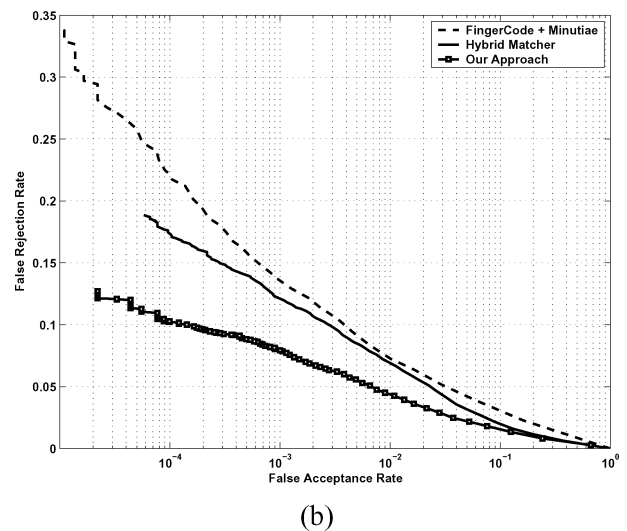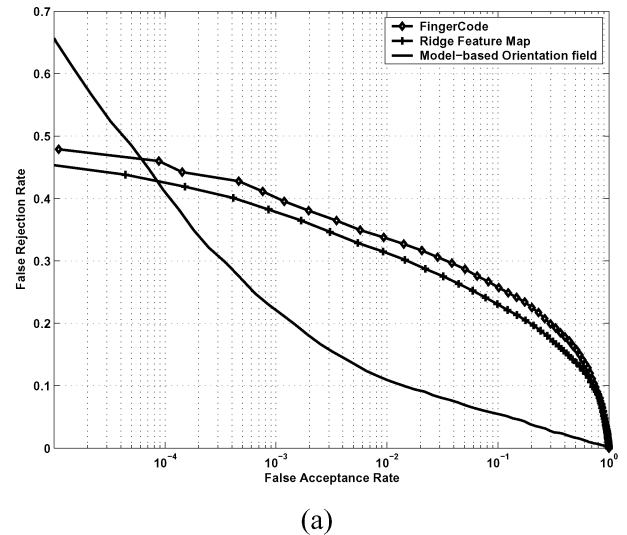

(a)

(b)

Fig. 11. Comparison with the previous works on the testing database of THUVLAB: (a) not combined with the minutiae-based matcher and (b) combined with the minutiae-based matcher.

TABLE III
COMPARISON WITH PREVIOUS WORKS

Methods	Performance (%)			Template Storage (byte)		Running Time (sec)	
	$FRR_{0.01\%}$	$FRR_{0.1\%}$	EER	Minutiae	Other Feature	Extraction	Matching
Minutiae	26.4%	17.4%	4.3%	240	—	0.03	0.002
FingerCode+Minutiae	22.1%	13.6%	4.4%	240	640	1.23	0.005
Hybrid Matcher	17.3%	12.1%	3.7%	240	1,800	1.23	0.005
Our Approach	10.2%	7.9%	2.9%	160	257	0.30	0.013

M, is set as 80, as shown in [1], [2], [7]. As for the *hybrid matcher*, there are eight ridge feature maps needed to be saved with size of 15×15. The storage for *FingerCode* is quoted from the original paper. It shows that our approach by combining the minutiae and the orientation field for recognition is better than the others for the performance and the template storage required, while holding a practical processing speed. Another advantage is that our approach can preserve the whole orientation field information in the feature template for further usage.

There are also failure cases for our system. Some typical examples are shown in Fig. 12. In these images, neither the minutiae nor the orientation field can be accurately estimated. None

Fig. 12. Several typical failure cases for recognitions, in which neither the minutiae nor the orientation field can be accurately estimated due to serious noises.

of the two kinds of features can be used to correctly verify the fingerprints. Some improvements can be made to make it adaptive to different situations. For example, the matching score for the orientation fields can be weighted by the variance within a block to account for the noisy orientation values occurring at some blocks. More accurate and robust alignment algorithm may also be helpful.

VI. OTHER APPLICATION: FINGERPRINT ALIGNMENT

In real systems, fingerprint images often suffer from translation, rotation, and slightly scaling transformation due to different pressures. Before matching two fingerprint impressions $\mathcal{A}$ and $\mathcal{B}$, it is necessary to register these two images to bring the features from $\mathcal{A}$ in the spatial proximity of their corresponding counterparts from $\mathcal{B}$. It is often assumed that scaling transformation does not need to be considered [6], [13]. Denote the geometrical transformation parameters with $[t_x, t_y, \phi]^T$ for the translation and rotation. After alignment, the point (x, y) and its orientation $O(x, y)$ will be mapped to the point (x', y') and $O'(x', y')$ as follows:

$$\begin{pmatrix} x' \\ y' \end{pmatrix} = \begin{pmatrix} \cos \phi & \sin \phi \\ -\sin \phi & \cos \phi \end{pmatrix} \begin{pmatrix} x \\ y \end{pmatrix} + \begin{pmatrix} t_x \\ t_y \end{pmatrix}$$

and

$$O'(x', y') = O(x, y) - \phi.$$

In this section, we propose to incorporate the global orientation field information into the fingerprint alignment stage. It is another application for the global structure of the fingerprints. Our approach is proved to be useful for the alignment between the fingerprints which are either incomplete or containing serious noises such as those latent prints left on the spot. It can be used to facilitate semi-automatic latent fingerprints recognition, or perform fingerprint mosaicking [32]. For the alignment between normal-quality fingerprints, our approach has similar performance with the conventional minutiae-based GHT method while taking much more time, and is not suitable for large-scale AFIS system.

A. Previous Fingerprint Alignment Methods

One kind of classical alignment algorithms is based on the minutiae points by GHT [4], [33]. For any minutiae pair from

two fingerprints, if the two minutiae points are in a predefined bounding box after transformation estimated by these points, it will add an evidence to the voting space. The optimal candidate in the voting space is the estimation of the alignment parameters.

Despite its simplicity, the minutiae-based alignment algorithm is limited in some situations. First, spurious minutiae points will degrade its performance seriously, which often occur in dry, snatchy fingerprints, or damp, blurred fingerprints. Since it is based on the voting strategy, spurious minutiae pairs will cause many *false votes* and *false peaks* in the Hough voting space, leading to the wrong transformation estimation. Second, in many situations, such as the fingerprints left on the spot or uncooperative users, the captured image is usually only a fingerprint fragment. In this case, the area of the common region and the number of the common minutiae points are relatively small, and thus it is difficult to accumulate enough evidence in the Hough transform space to find the genuine optimal geometric transformation.

Some other algorithms used some more global structures to do alignment rather than the individual local minutiae points. Jain *et al.* [5] proposed to align the minutiae pairs by the correlation between the two ridges from the minutiae pairs, instead of comparing with their positions and angles as the conventional method. Eshera and Sanders [34] proposed to construct an attributed star-like graph where branches constitute nearest neighbor minutiae. The fingerprint pairs are aligned and matched by comparing the star-like graphs.

B. Proposed Alignment Method Based on Orientation Field

The proposed alignment method is mainly based on the global orientation field while using the minutiae to select the initial candidate transformations. First, we perform the conventional minutiae-based GHT algorithm. Instead of finding the unique optimal candidate in the voting space, we keep top-K candidates. The best one is selected with the largest matching score, which is defined as the product of the voting value and the similarity between the orientation fields $O_\mathcal{A}$ and $O_\mathcal{B}$ after transformation. It is proved to be useful for those poor-qualitied fingerprints with many spurious minutiae or small common region, keeping a practical speed for real systems. In our study we choose $K = 300$ empirically. The definition of the similarity $S(\mathcal{A}, \mathcal{B})$ can be referred as (8).

Some results are shown in Figs. 13 and 14. In Fig. 13(a) and (b), two fingerprints are captured from the same finger at different time. One of them is damp and blurred at the bottom and contains many spurious minutiae. The other is incomplete and also very noisy. We show the extracted minutiae and orientation fields in Fig. 13(c)–(f). The alignment result with the minutiae-based method and the result with the orientation field based method are shown in Fig. 13(g) and (h), respectively. In order to illustrate the correctness of the alignment results, we manually labeled two corresponding points (marked as the red circle and the blue square) in the images, and the two images are blended after geometrical transformation. In Fig. 14, an on-the-spot fingerprint and another good-quality print of the same finger are shown in Fig. 14(a) and (b). After aligned by the
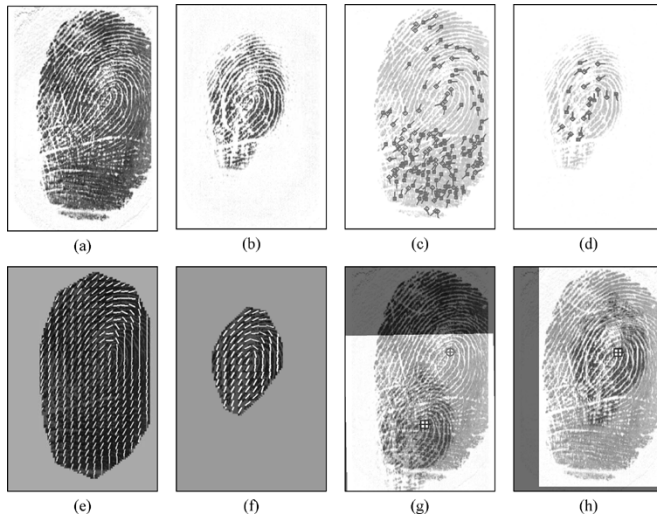
Fig. 13. Fingerprint alignment with the minutiae-based method and the orientation-field-based method: (a) and (b) are the original images, (c) and (d) are the extracted minutiae, and (e) and (f) are the corresponding orientation fields. (g) shows the alignment result based on the minutiae method, while (h) shows the alignment result based on the proposed method. The corresponding point pairs (manually labeled) are marked as the red circle and the blue square [they are overlapped in (h)].
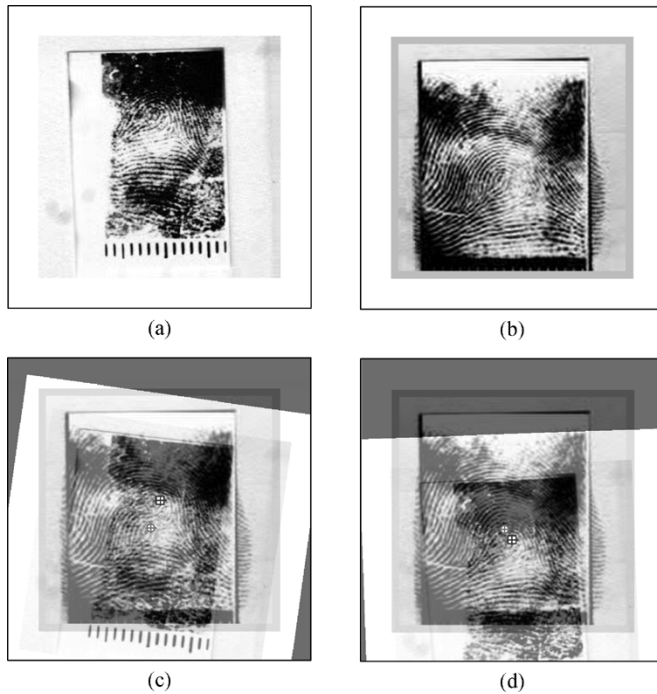

Fig. 14. Live fingerprints cases. (a) the live fingerprint left on the spot; (b) the good-quality print from the same finger; (c) the alignment result based on the minutiae based method; and (d) the alignment result based on the proposed method. The corresponding point pairs (manually labeled) are marked as the red circle and the blue square.

minutiae based method and the orientation field based method, the results are shown in Fig. 14(c) and (d), respectively. It shows that our approach outperforms the conventional minutiae-based method when the fingerprint's quality is poor.

To verify the effectiveness of our proposed alignment method for the poor-qualited or incomplete fingerprints statistically, we have conducted some experiments on a subset of THUVLAB

TABLE IV
COMPARISON FOR FINGERPRINT ALIGNMENT

	Minutiae	Ridge Correlation	Our Approach
Error Rate	63%	71%	49%
$\overline{\delta}_\phi$ (radian)	0.26	0.22	0.20
$\overline{\delta}_{t_x}$ (pixel)	51	61	43
$\overline{\delta}_{t_y}$ (pixel)	60	75	45
Cost Time (sec)	0.05	0.03	0.85

which consists of 100 selected poor-qualited fingers (two prints for each finger, and thus 200 fingerprints). These images includes the incompleteness or noises like smudges, scars, and creases, which have similar or worse quality as the bottom row in Fig. 7. Each pair from the same finger is manually aligned beforehand. The computed transformation parameters are used as the ground truth.

We have made comparisons with the minutiae-based method and the alignment algorithm in [5] named as *Ridge Correlation*. The estimated transformation, $(\hat{t}_x, \hat{t}_y, \hat{\phi})$, is compared with the ground truth, $(t_x^{(0)}, t_y^{(0)}, \phi^{(0)})$. If the differences are less than the predefined thresholds, the estimation is considered as *correct*, otherwise *wrong*. The thresholds are set as $\Delta_{t_x} = \Delta_{t_y} = 16$ pixels, and $\Delta_\phi = 0.15$, which is similar as the criteria of human inspection. The results are shown in Table IV for the three alignment methods including the error rate (define as the percentage of *wrong* alignment), the average running time, and the average difference of the estimated transformations with the ground truth. Since *ridge correlation* depends on the best-matched minutiae pair, it is easy to select the false pair considering a lot of spurious minutiae in the poor-qualited images, and thus it does not perform well in this experiment. Our approach has satisfactory performance. It proves that the global orientation field is helpful for the alignment, especially for the poor-qualited fingerprint images while it takes much more time. One possible application is to facilitate semi-automatic latent fingerprints recognition.

VII. SUMMARY AND DISCUSSIONS

In this paper, we present a framework for fingerprint recognition by combining the global structure (the model-based orientation field) and the local cues (minutiae). The fingerprint representation takes less than 420 bytes to save the orientation field, the minutiae, the singular points and the effective region mask. An ensemble classifier is constructed using the orientation field and the minutiae as features for fingerprint matching. Experimental results show that our proposed method is better than the conventional minutiae-based method and the previous works which also use some complementary information for matching. We can also conclude that the model-based reconstructed orientation field is more robust and discriminative than the original orientation field while it needs few bytes to store. It can be used for further fingerprint processing, matching or indexing.

Besides, we proposed a novel fingerprint alignment method with the minutiae and the orientation field. This method, while

taking much more time, is effective for poor-qualitied finger-prints or incomplete fragments of fingerprints. It can be used to facilitate semi-automatic latent fingerprints recognition.

Representing fingerprints with a complete set of complementary features is not only important for storing but also very helpful for recognition. The global-and-local representation framework can be extended further to include some other global or local features available in the fingerprint images such as the ridge density map. From a scientific view, the performance limit of the fingerprint matching algorithm is determined by fingerprint individuality. Previous works, such as [7] and [8], have proposed some models to estimate the individuality of the fingerprints assuming that each minutiae is independent with positions and orientations. The assumption, however, is not completely correct, since the orientations of the minutiae are actually related to each other because they are determined by the global ridge patterns. Using the whole orientation field as a kind of discriminant feature is helpful to estimate the individuality more precisely. Furthermore, we believe incorporating the whole orientation field into matching stage can reinforce the individuality of fingerprints.

ACKNOWLEDGMENT

REFERENCES

[1] D. Maltoni, D. Maio, A. K. Jain, and S. Probhaker, *Handbook of Fingerprint Recognition*. New York: Springer-Verlag, 2003.

[2] A. K. Jain, R. Bolle, and S. Pankanti, *BIOMETRICS: Personal Identification in Networked Society*. New York: Kluwer, 1999.

[3] Legal challenges to fingerprints [Online]. Available: http://onin.com/fp/daubert_links.html

[4] N. K. Ratha, K. Karu, S. Chen, and A. K. Jain, "A real-time matching system for large fingerprint databases," *IEEE Trans. Pattern Anal. Mach. Intell.*, vol. 18, no. 8, pp. 799–813, Aug. 1996.

[5] A. K. Jain and L. Hong, "On-line fingerprint verification," *IEEE Trans. Pattern Anal. Mach. Intell.*, vol. 19, no. 4, pp. 302–314, Apr. 1997.

[6] A. K. Jain, S. Prabhakar, L. Hong, and S. Pankanti, "Filterbank-based fingerprint matching," *IEEE Trans. Image Process.*, vol. 9, no. 5, pp. 846–859, May 2000.

[7] S. Pankanti, S. Prabhakar, and A. K. Jain, "On the individuality of fingerprints," *IEEE Trans. Pattern Anal. Mach. Intell.*, vol. 24, no. 8, pp. 1010–1025, Aug. 2002.

[8] X. Tan and B. Bhanu, "On the fundamental performance for fingerprint matching," in *Proc. IEEE Computer Society Conf. Computer Vision and Pattern Recognition*, vol. 2, Jun. 2003, pp. 499–504.

[9] Q. Xiao and Z. Bian, "An approach to fingerprint identification by using the attributes of feature lines of fingerprint," in *Proc. Int. Conf. Pattern Recognition*, 1986, pp. 663–665.

[10] A. J. Willis and L. Myers, "A cost-effective fingerprint recognition system for use with low-quality prints and damaged fingertips," *Pattern Recognit.*, vol. 34, no. 2, pp. 255–270, 2001.

[11] A. Crouzil, L. Massip-Pailhes, and S. Castan, "A new correlation criterion based on gradient fields similarity," in *Proc. Int. Conf. Pattern Recognition*, 1996, pp. 632–636.

[12] T. Hatano, T. Adachi, S. Shigematsu, H. Morimura, S. Onishi, Y. Okazaki, and H. Kyuragi, "A fingerprint verification algorithm using the differential matching rate," in *Proc. Int. Conf. Pattern Recognition*, vol. 3, 2002, pp. 799–802.

[13] M. Tico and P. Kuosmannen, "Fingerprint matching using an orientation-based minutia descriptor," *IEEE Trans. Pattern Anal. Mach. Intell.*, vol. 25, no. 8, pp. 1009–1014, Aug. 2003.

[14] A. Ross, A. Jain, and J. Reisman, "A hybrid fingerprint matcher," *Pattern Recognit.*, vol. 36, no. 7, pp. 1661–1673, 2003.

[15] L. Hong, Y. Wan, and A. K. Jain, "Fingerprint image enhancement: Algorithm and performance evaluation," *IEEE Trans. Pattern Anal. Mach. Intell.*, vol. 20, no. 8, pp. 777–789, Aug. 1998.

[16] R. Cappelli, A. Lumini, D. Maio, and D. Maltoni, "Fingerprint classification by directional image partitioning," *IEEE Trans. Pattern Anal. Mach. Intell.*, vol. 21, no. 5, pp. 402–421, May 1999.

[17] B. Sherlock and D. Monro, "A model for interpreting fingerprint topology," *Pattern Recognit.*, vol. 26, no. 7, pp. 1047–1055, 1993.

[18] P. Vizcaya and L. Gerhardt, "A nonlinear orientation model for global description of fingerprints," *Pattern Recognit.*, vol. 29, no. 7, pp. 1221–1231, 1996.

[19] J. Zhou and J. Gu, "Modeling orientation fields of fingerprints with rational complex functions," *Pattern Recognit.*, vol. 37, no. 2, pp. 389–391, Feb. 2004.

[20] J. Gu, J. Zhou, and D. Zhang, "A combination model for orientation field of fingerprints," *Pattern Recognit.*, vol. 37, no. 3, pp. 543–553, Mar. 2004.

[21] J. Zhou and J. Gu, "A model-based method for the computation of fingerprints' orientation field," *IEEE Trans. Image Process.*, vol. 13, no. 6, pp. 821–835, Jun. 2004.

[22] A. M. Bazen, "Systematic methods for the computation of the directional fields and singular points of fingerprints," *IEEE Trans. Pattern Anal. Mach. Intell.*, vol. 24, no. 7, pp. 905–919, Jul. 2002.

[23] A. K. Jain, S. Prabhakar, and L. Hong, "A multichannel approach to fingerprint classification," *IEEE Trans. Pattern Anal. Mach. Intell.*, vol. 21, no. 4, pp. 348–359, Apr. 1999.

[24] K. Karu and A. K. Jain, "Fingerprint classification," *Pattern Recognit.*, vol. 17, no. 3, pp. 389–404, 1996.

[25] J. Kittler, M. Hatef, R. P. W. Duin, and J. Matas, "On combining classifiers," *IEEE Trans. Pattern Anal. Mach. Intell.*, vol. 20, no. 3, pp. 226–239, Mar. 1998.

[26] T. K. Ho, J. J. Hull, and S. N. Srihari, "Decision combination in multiple classifier systems," *IEEE Trans. Pattern Anal. Mach. Intell.*, vol. 16, no. 1, pp. 66–75, Jan. 1994.

[27] S. Prabhakar and A. K. Jain, "Decision-level fusion in fingerprint verification," *Pattern Recognit.*, vol. 35, pp. 861–874, 2002.

[28] C. M. Bishop, *Neural Networks for Pattern Recognition*. Oxford, U.K.: Oxford Univ. Press, 1995.

[29] R. O. Duda and P. E. Hart, *Pattern Classification and Scene Analysis*. New York: Wiley, 1973.

[30] 94 704J. A. Bilmes, "A Gentle Tutorial of the Em Algorithm and its Application to Parameter Estimation for Gaussian Mixture and Hidden Markov Models," Int. Comput. Sci. Inst., Berkeley, CA, Tech. Rep. TR-97-021, Apr. 1998.

[31] D. Maio, D. Maltoni, R. Cappelli, J. L. Wayman, and A. K. Jain, "Fvc2000: Fingerprint verification competition," *IEEE Trans. Pattern Anal. Mach. Intell.*, vol. 24, no. 3, pp. 402–412, Mar. 2002.

[32] A. K. Jain and A. Ross, "Fingerprint mosaicking," presented at the Int. Conf. Acoustic Speech and Signal Processing, May 2002.

[33] G. Stockman, S. Kopstein, and S. Benett, "Matching images to models for registration and object detection via clustering," *IEEE Trans. Pattern Anal. Mach. Intell.*, vol. PAMI-4, no. 3, pp. 229–241, Mar. 1982.

[34] M. A. Eshera and R. E. Sanders, "Fingerprint Matching System," U.S. Patent 5613014, 1997.

Jinwei Gu (S'05) was born in 1980. He received the B.S. degree from the Department of Automation, Tsinghua University, Beijing, China, in 2002, where he is currently pursuing the M.S. degree.

His research interests are in pattern recognition, computer vision, and intelligent information processing. He has published four papers in international journals and two papers in international conferences.

Jie Zhou (M'01–SM'04) was born in 1968. He received the B.S. and M.S. degrees from the Department of Mathematics, Nankai University, Tianjin, China, in 1990 and 1992, respectively, and the Ph.D. degree from the Institute of Pattern Recognition and Artificial Intelligence, Huazhong University of Science and Technology (HUST), Wuhan, China, in 1995.

From 1995 to 1997, he was a Postdoctoral Fellow with the Department of Automation, Tsinghua University, Beijing, China. Currently, he is a Full Professor and Assistant Chair with the Department of Automation, Tsinghua University. His research area includes pattern recognition, image processing, computer vision, and information fusion. Recently, he has authored more than ten papers in international journals and more than 40 papers in international conferences. He is an associate editor for the *International Journal of Robotics and Automation*.

Dr. Zhou received the Best Doctoral Thesis Award from HUST, the First Class Science and Technology Progress Award from the Ministry of Education, China, and the Excellent Young Faculty Award from Tsinghua University in 1995, 1998, and 2003, respectively.

Chunyu Yang was born in 1982. He received the B.S. degree from the Department of Automation, Tsinghua University, Beijing, China, in 2004, where he is currently pursuing the M.S. degree.

His research interests are in pattern recognition, computer vision, machine learning, and intelligent information processing.